



**HAL**  
open science

## Fabrication of n-Type Doped V-Shaped Structures on (100) Diamond

Christoph Schreyvogel, Solange Temgoua, Christian Giese, Volker Cimalla, Julien Barjon, Christoph Erwin Nebel

► **To cite this version:**

Christoph Schreyvogel, Solange Temgoua, Christian Giese, Volker Cimalla, Julien Barjon, et al.. Fabrication of n-Type Doped V-Shaped Structures on (100) Diamond. *physica status solidi (a)*, 2021, 218 (7), 10.1002/pssa.202000502 . hal-03218440

**HAL Id: hal-03218440**

**<https://hal.science/hal-03218440>**

Submitted on 1 Jun 2021

**HAL** is a multi-disciplinary open access archive for the deposit and dissemination of scientific research documents, whether they are published or not. The documents may come from teaching and research institutions in France or abroad, or from public or private research centers.

L'archive ouverte pluridisciplinaire **HAL**, est destinée au dépôt et à la diffusion de documents scientifiques de niveau recherche, publiés ou non, émanant des établissements d'enseignement et de recherche français ou étrangers, des laboratoires publics ou privés.



Distributed under a Creative Commons Attribution 4.0 International License

# Fabrication of n-Type Doped V-Shaped Structures on (100) Diamond

Christoph Schreyvogel,<sup>\*</sup> Solange Temgoua, Christian Giese, Volker Cimalla, Julien Barjon, and Christoph. E. Nebel

Herein, a technological process for the fabrication of n-type doped V-shaped structures on (100) single-crystalline diamond substrates, designed to overcome the limitations of n-type doping on (100) surfaces, is presented. This doping enhancement process can be applied to realize electronic power devices such as a junction barrier Schottky diode or junction field effect transistors with low on-resistance. Herein, a catalytic etching process is performed by using square-shaped nickel masks on the diamond surface and annealing in a hydrogen atmosphere, resulting in the formation of inverted pyramidal structures with flat {111} sidewalls. The resulting V-shaped structures are subsequently overgrown with phosphorus-doped diamond to achieve n-type doped facets with higher doping concentrations. Cathodoluminescence studies reveal the predominant incorporation of phosphorus donors on the {111} sidewalls of V-shaped structures.

## 1. Introduction

Diamond has outstanding physical and electronic properties, rendering it an attractive material for fabricating next-generation wide-bandgap devices. Today, through microwave plasma-enhanced chemical vapor deposition, growing high-quality intrinsic, n-type and p-type diamond films is possible, enabling the realization of both unipolar (e.g., Schottky diode) and bipolar (e.g., pin diode) devices.<sup>[1–3]</sup> For doping diamond, phosphorus (P) and boron (B) are used as n-type and p-type dopants, respectively, i.e., phosphorus is considered as a donor and boron as an

acceptor.<sup>[4]</sup> In 1997, Koizumi et al.<sup>[5]</sup> were the first to demonstrate the homoepitaxial growth of n-type layers on (111) diamond by adding a phosphorus precursor to the CH<sub>4</sub>/H<sub>2</sub> gas mixture in the growth chamber. Since then, phosphorus has been the most promising dopant for realizing n-type diamond. Almost a decade after this discovery, n-type doping of (100)-oriented diamond has been established.<sup>[6]</sup> This achievement marked an important step because (100) diamond offers many advantages compared with (111) diamond, such as with respect to polishing, crystal defect densities, and size upscaling.<sup>[7]</sup> Meanwhile, wafer-size (100) diamond larger than 3 in. has been demonstrated by heteroepitaxial growth.<sup>[8]</sup> Therefore, for the development of future power devices, (100)-oriented dia-

mond is preferred. Although many unipolar and bipolar power devices have been developed since then, the full performance potential of these devices has yet to be realized, partially because of the high resistivity of n-type doped diamond films, which increases the serial resistance and degrades Ohmic contacts. One reason for this is that, for (100) diamond, the P incorporation efficiency is very low, approximately two orders of magnitude smaller than that of (111) diamond. In addition, electrically inactive or acceptor-like defect states compensate for the n-type doping.<sup>[4,9,10]</sup> Despite numerous theories, the exact nature of those compensating defects still need to be experimentally elucidated.


Therefore, improving the electronic properties of n-type doped (100) diamond, especially to achieve heavily P-doped layers, presents a challenge. Furthermore, despite achieving lower n-type doping concentrations using (100) diamond, we get improvements to the Hall mobility and the crystal quality,<sup>[11]</sup> which is another advantage of this crystal orientation for the fabrication of power devices.

Different methods have been proposed in the literature for improving the electrical contacts on n-type layers on (100) diamond. One example is the partial graphitization of the n-type surface to reduce the potential barrier between the n-type layer and the metal contact.<sup>[12]</sup> Another example is the selective growth of a highly P-doped layer on (100) diamond in the (111) growth direction. To achieve this, U-shaped patterns were fabricated by inductively coupled plasma etching, which initiated the (111) growth in the corners at the bottom of U-shaped pattern.<sup>[13]</sup>

Unlike silicon, no wet-chemical etching processes are known for the fabrication of V-shaped structures on diamond.

Dr. C. Schreyvogel, Dr. C. Giese, Dr. V. Cimalla, Dr. C. E. Nebel  
Fraunhofer IAF  
Institute for Applied Solid State Physics  
79108 Freiburg, Germany  
E-mail: christoph.schreyvogel@iaf.fraunhofer.de

Dr. S. Temgoua, Dr. J. Barjon  
Groupe d'Etude de la Matière Condensée (GEMAC)  
Université Saint-Quentin en Yvelines  
Versailles 78000, France

 The ORCID identification number(s) for the author(s) of this article can be found under <https://doi.org/10.1002/pssa.202000502>.

© 2021 The Authors. physica status solidi (a) applications and materials science published by Wiley-VCH GmbH. This is an open access article under the terms of the Creative Commons Attribution License, which permits use, distribution and reproduction in any medium, provided the original work is properly cited.

DOI: 10.1002/pssa.202000502

In general, plasma etching processes, such as reactive ion etching with metal masks on the diamond surface, are used.<sup>[14,15]</sup> However, owing to the etching mechanism, this process cannot create V-shaped structures with well-defined {111} facets as sidewalls. In addition, the plasma process generates defects and roughness on the diamond surface, which impairs overgrowth and degrades the device performance, for example, by reducing the carrier mobility and lowering the breakdown voltage. To achieve the necessary V-shaped structure with {111} facets as sidewalls, an alternative, non-plasma etching method that has high anisotropy and generates fewer defects is required. It is well known that diamond can be etched catalytically by using a metal mask on the diamond surface and exposing it to a hydrogen ( $H_2$ ) atmosphere at elevated temperatures.<sup>[16–18]</sup> This catalytic etching is based on a thermochemical solid-solution reaction between the metal film on the diamond surface and the carbon atoms in the diamond lattice, followed by the subsequent gasification of the dissolved carbon in the metal film. Efficient etching requires a metal with a high carbon solubility. Metals satisfying this requirement include nickel (Ni), cobalt (Co), and platinum (Pt), of which Ni and Pt have the highest and lowest carbon solubilities, respectively.<sup>[19]</sup>

Recently, Temahuki et al.<sup>[20]</sup> demonstrated the fabrication of such microstructures by catalytic etching with Ni nanoparticles. The subsequent overgrowth of those structures using highly phosphorus-doped diamond notably improved the Ohmic contact properties to the n-type doped diamond on a (100) substrate. While this process forms structures with irregular sizes and positions, for electronic device fabrication, it is recommended that the shape, size, and position of the V-shaped pattern are controlled.

In this article, we present a process for fabricating defined V-shaped structures on a (100) diamond surface, which has {111} facets that can be overgrown subsequently with an n-type layer. Furthermore, using cathodoluminescence (CL), we demonstrate the predominant incorporation of phosphorus donors on the {111} sidewalls.

## 2. Results and Discussion

### 2.1. Catalytic Etching to Produce V-Shapes with {111} Facets

#### 2.1.1. Basic Mechanism of Catalytic Etching of Diamond

Figure 1 shows a schematic representation of the basic mechanisms involved in the catalytic etching process. Although it

remains to be elucidated fully, we describe here our current understanding of the etching mechanism. Further details can also be found in the literature.<sup>[16–18]</sup> A diamond sample with a Ni film on the surface was exposed at elevated temperatures ( $850^\circ\text{C}$  in this case) to a hydrogen atmosphere. The bonds between C atoms in the diamond lattice at the interface to the Ni film were broken, while the Ni film catalytically dissociated gaseous hydrogen molecules into hydrogen atoms. Owing to the concentration gradient of each constituent in the Ni film, C atoms diffused toward the interface of the Ni film–hydrogen atmosphere, while hydrogen atoms diffused toward the interface of the Ni film–diamond surface. Hydrogen atoms in the film subsequently gasified the dissolved carbon atoms, leading to the formation of methane ( $\text{CH}_4$ ) or other hydrocarbon complexes ( $\text{C}_x\text{H}_y$ ). These hydrocarbon molecules diffused out of the Ni film and desorbed. These steps were repeated continuously, and thus this mechanism was responsible for the constant release of dissolved C in the Ni film, preventing the saturation of C in the Ni film and promoting the ongoing etching of diamond. As the Ni film breaks the covalent bonds of the C atoms in the diamond lattice, we have to consider the bonding between the C atoms within different crystal planes. The {111} planes are the closest packed planes; therefore, C atoms in these planes are strongly bound. Consequently, these planes are more resistant to the dissolution of C atoms in the diamond lattice.<sup>[21]</sup> On (100) diamond, etch pits resembling (truncated) inverted pyramids with four {111} planes as sidewalls were formed. This etching anisotropy observed for diamond is comparable with the chemical etching of silicon with KOH solutions.

This theory of etching mechanism, which is described above, can be deduced from the following experimental evidences published in the literature and summarized in the following.<sup>[17,18]</sup> First of all, when a diamond film with a Ni mask on the surface is annealed in vacuum, i.e., without a hydrogen atmosphere, there is no desorption of carbon dissolved in the Ni film. This leads to the formation of a nucleated carbon layer in the Ni film measured with energy dispersive X-ray analysis (EDX). This carbon layer results in stopping of the catalytic etching activity proving that hydrogen is required for a removal of carbon dissolved in Ni. By adding a hydrogen atmosphere, the chemical composition of the exhaust gas of the annealing oven was investigated with a quadrupole mass spectrometer, proving that methane is the main hydrocarbon species produced during the catalytic etching procedure. Furthermore, the higher the pressure of hydrogen gas in the oven, the higher is the etching

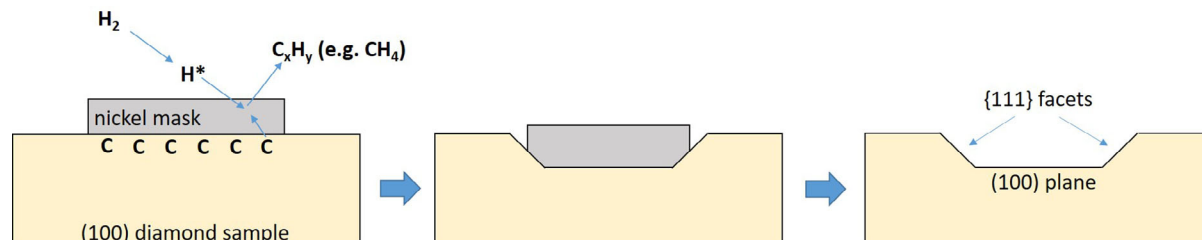


**Figure 1.** Schematic representation of the basic mechanisms involved in a catalytic etching process. A catalytic dissolution of carbon atoms in the diamond lattice by the Ni mask and the subsequent gasification of the dissolved carbon atoms by the hydrogen atoms (formation of hydrocarbon molecules) leads to the formation of an inverted (truncated) pyramidal (V-shaped) structure with {111} facets.

of diamond due to enhancement of catalytically generated atomic hydrogen and desorption of carbon (hydrocarbon molecules).

There are two different theories with respect to the formation of gaseous hydrocarbon species. One theory is that due to the concentration gradient of each constituent in the Ni film, C atoms diffused toward the interface of the Ni film–hydrogen atmosphere, while hydrogen atoms diffused toward the interface of the Ni film–diamond surface and hence gas is produced within the Ni film. The other theory is that dissolved carbon diffuses to the interface of the metal–hydrogen atmosphere where gaseous hydrocarbon molecules like methane are formed. It still remains to be experimentally elucidated which mechanism is the dominant one.

The surface chemistry of the catalytically etched diamond sample as well as of the Ni film was analyzed with X-ray photoelectron spectroscopy (XPS) and EDX, which did not show the existence of nickel carbide (NiC)—neither at the interface of the Ni film and diamond nor in the Ni film. NiC would limit the etching process. This finding might be supported by the fact that NiC becomes unstable at temperatures above 350 °C.

### 2.1.2. Fabrication of {111} Facets

In this experiment, we performed a catalytic etching on our sample for 2 h before the wet-chemical removal of the Ni masks. Two types of etched diamond shapes were observed via scanning electron microscope (SEM), as shown in **Figure 2**. For the parallel alignment of the Ni mask edges to the  $\langle 110 \rangle$  crystallographic direction of the diamond substrate, we obtained well-shaped inverted and truncated pyramids with smooth {111} facets as

sidewalls and a (100) plane at the bottom (Figure 2b,c, left). In contrast, for the parallel alignment of the Ni mask edges to the  $\langle 100 \rangle$  crystallographic direction of the diamond substrate, smooth sidewalls corresponding to {111} facets were obtained in the corner of the trench structure only, with the other sidewalls showing rough and jagged profiles which are indicated as {101} facets (Figure 2b,c, right). The roughness of {101} facets might be due to lower resistance to etching compared with {111} planes causing a partial etching into that facet. These results indicate that the alignment of the Ni mask relative to the crystal planes of the diamond sample is critical for achieving controlled V-shaped structures. Experiments by other research groups, which used Ni nanoparticles on the diamond surface, showed that the Ni-etched microstructures self-aligned along the  $\langle 110 \rangle$  crystallographic direction of the diamond.<sup>[16,17,20]</sup> This explains the observed difference in the shape of the trench structures for different Ni mask alignments. The angle between the {111} sidewalls of the inverted pyramids and the (100) surface is  $\approx 55^\circ$ ,<sup>[22]</sup> which was confirmed by atomic force microscope (AFM) measurements (not shown here). Similarly, publications from other research groups showed that the sidewalls are {111} facets.<sup>[16,21,23]</sup> After 2 h of etching, the white light interferometer (WLI)-measured depth of these etched structures was  $\approx 1\text{--}1.2\ \mu\text{m}$ , corresponding to an etching rate of  $\approx 0.5\text{--}0.6\ \mu\text{m h}^{-1}$ . In addition, the size of the etched structures corresponded to the size of the Ni masks deposited initially, which enables us to define the final size of these structures accurately.

Increasing the duration of the catalytic etching process to 6 h had no qualitative effect on the characteristics of the final structures. Quantitatively, the only change was an increase in the depth of the etched structures (i.e., the inverted pyramids and

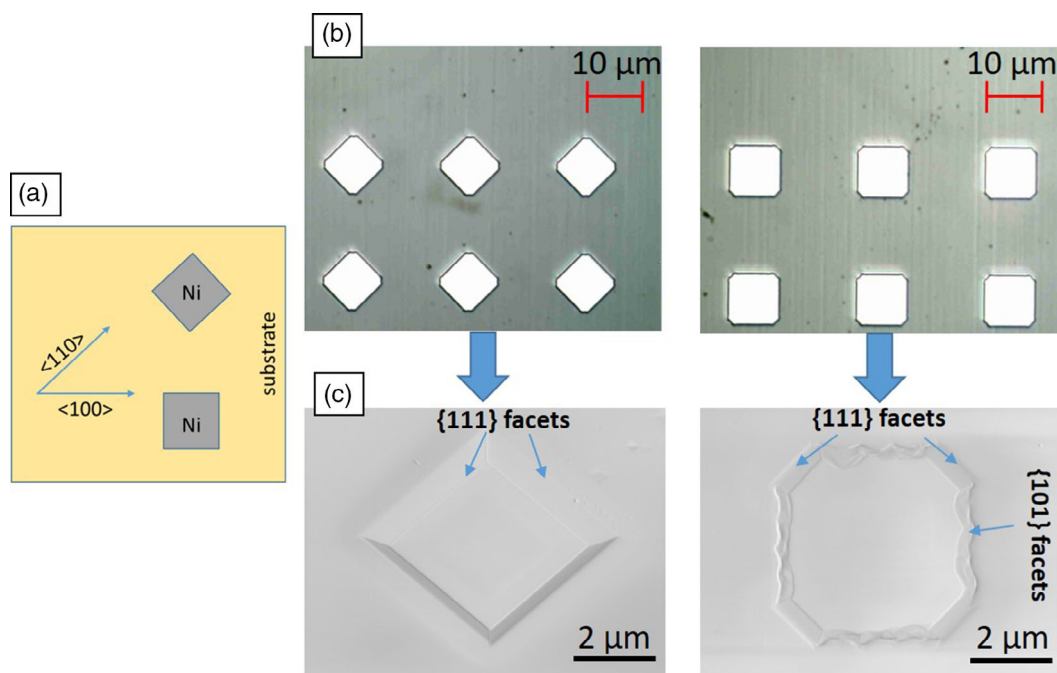


**Figure 2.** Deposition of Ni masks and catalytic etching after 2 h. a) Alignment of the Ni masks with respect to the  $\langle 100 \rangle$  or  $\langle 110 \rangle$  crystallographic direction of the diamond sample. b) Microscope images of the deposited Ni masks ( $10 \times 10\ \mu\text{m}$ ) and c) SEM images after the etching and the wet-chemical removal of Ni ( $5 \times 5\ \mu\text{m}$ ) for the two differently aligned masks.

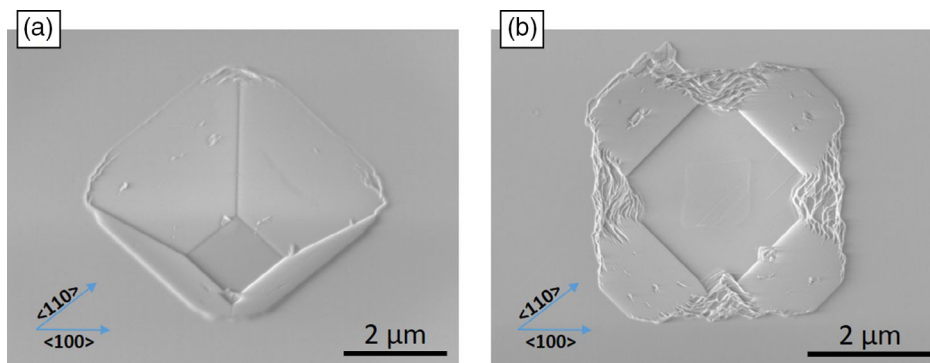


**Figure 3.** SEM images of diamond surface after 6 h of catalytic etching. a) Perfect inverted truncated pyramids for a Ni mask aligned along the  $\langle 110 \rangle$  crystallographic direction and b) square-shaped trench structures with smooth sidewalls in the corners only for a Ni mask aligned along the  $\langle 100 \rangle$  crystallographic direction.

trenches), as shown in **Figure 3a,b**. In this case, the structures were  $\approx 3.6\text{--}4.5\ \mu\text{m}$  deep, which corresponds to an etching rate of  $0.6\text{--}0.75\ \mu\text{m h}^{-1}$ . Owing to the larger depth of these structures, the features appear more pronounced.

The square shape of the etched structures and emergence of  $\{111\}$  facets (i.e., tilted sidewalls) indicated that the catalytic etching of the diamond surface with Ni is indeed anisotropic, with the  $\{111\}$  facets acting as etch-stop planes. This anisotropic etching also seems to remove the defects from the  $(100)$  surface of the diamond sample because the bottom of the etched structure appears smoother than the area of the surface, which has not been exposed to Ni etching.

## 2.2. Overgrowth of $\{111\}$ Facets with n-Type Diamond

The morphology of these overgrown structures, measured by SEM and AFM, is shown in **Figure 4**. Following overgrowth,

the shape of the truncated inverted pyramids appeared to be very similar (**Figure 4a**). As can be observed clearly, these structures showed extremely smooth  $\{111\}$  side facets with a smaller area of the  $(100)$  bottom (compared with the area before overgrowth), which indicates that the growth rate on the  $\{111\}$  facets was higher than that of the  $(100)$  plane. For the trench structures, the overgrowth procedure prompted the appearance of “umbrella-patterned” structures (**Figure 4b**). These structures showed an increased number of crystallographic facets, namely, smooth  $\{111\}$  facets at the corner and less smooth  $\{101\}$  facets along the edges of the former Ni mask. The depth of both n-type doped structures decreased to  $4\text{--}4.5\ \mu\text{m}$ , indicating that the growth rate on the  $\{111\}$  facets was higher than that for the  $(100)$  plane.

AFM measurements of the angle  $\alpha$  between the  $(100)$  surface and the sidewalls of both n-type doped structures were deduced from profiles along the  $\langle 110 \rangle$  directions (**Figure 4c,d**). Measurements acquired from 21 overgrown structures revealed

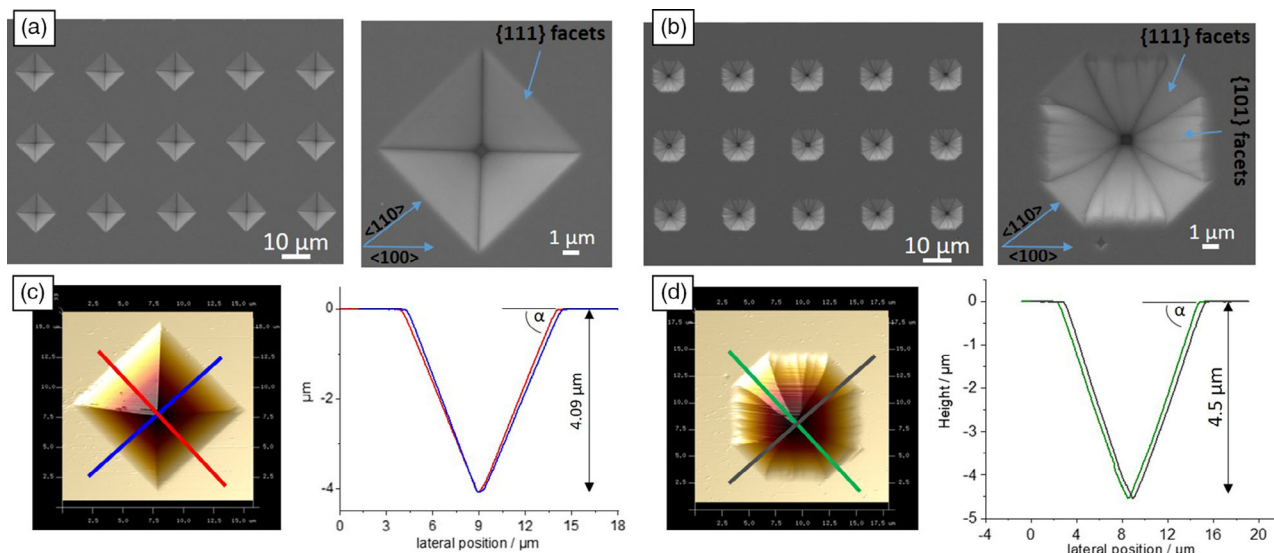


**Figure 4.** Resulting structures after overgrowth with a phosphorus-doped film. SEM overview images of a) inverted pyramid structures and b) umbrella-patterned structures with their corresponding c,d) AFM images of a single structure, from which the depth and angles of the facets were measured along the lines highlighted.

the mean angle values of  $54.3 \pm 1.9^\circ$  and  $54.6 \pm 1.0^\circ$ , respectively, for the inverted pyramidal and the umbrella-patterned structures. These results were consistent with the crystallographic angle of  $54.74^\circ$  between the  $\{100\}$  and  $\{111\}$  planes; thus, the sidewalls were oriented almost perfectly to the  $\{111\}$  plane post-growth. The angle  $\alpha$  between the (100) surface and the sidewalls along the  $\langle 100 \rangle$  axes, averaged across the measurements of 35 umbrella-patterned structures, was  $40.8 \pm 0.6^\circ$ . This value is close to  $45^\circ$ , which we would expect for a  $\{101\}$  facet. The observed deviation from the theoretical value is most probably caused by the rough starting morphology post-etching, which can influence the overgrowth in this direction. Indeed, this plane appears to be rougher than the  $\{111\}$  facets and has more defects.

### 2.3. CL Studies

CL spectra were measured both for the  $\{111\}$  facets of the inverted pyramidal structures and the (100) surface of the sample (spots P1, P2, and P3 in Figure 5a). Details of the energies and wavelengths of free and bound exciton lines as well as the approach for determining the doping concentration were reported by Barjon et al.<sup>[24]</sup>

In the CL spectrum corresponding to spot P3, which pertains to the (100) surface, the phosphorus-bound exciton was not detected. Here, we observed only a weak free exciton line,

$X_{TO}$  (Figure 5b). In contrast, when we measured CL spectra on spots P1 and P2, pertaining to the  $\{111\}$  facets of the inverted pyramidal structure, we detected both the free exciton line  $X_{TO}$  and the phosphorus-bound excitons  $P^0X_{TO}$ , as well as the boron-bound excitons  $B^0X_{TO}$  (Figure 5c). The existence of bound excitons in the spectra indicates the presence of phosphorus and boron as isolated impurities in the neutral state on substitutional sites in a rather high-quality crystalline lattice.<sup>[23,24]</sup>

As neither phosphorus- nor boron-bound excitons were visible for the (100) surface, we assume that the P-doped layer grown on the (100) plane is extremely thin and the doping level is below detection limit. These findings are supported by the facts that both the growth rate and the doping efficiency (for phosphorus and boron as well) on a (100) plane are much lower than that on a  $\{111\}$  facet.<sup>[4,25]</sup> The measurement of the visible spectral range provides further support because only on spot P3 the color center H3 (di-nitrogen-vacancy center, N–V–N),<sup>[26]</sup> which typically originates from Ib high-pressure and high-temperature (HPHT) substrates, is observed (Figure 5d). From the aforementioned findings, we can deduce that, for our growth conditions, the so-called alpha-parameter ( $\alpha$ -parameter) was small.<sup>[27,28]</sup> As demonstrated by Temahuki et al.,<sup>[20]</sup> this indicates the high selectivity of the growth of an n-type layer on the  $\{111\}$  facets compared with the (100) surface.

As phosphorus is considered as a donor and boron as an acceptor, in the following we label the (phosphorus) donor concentration as  $N_D$  and the (boron) acceptor concentration

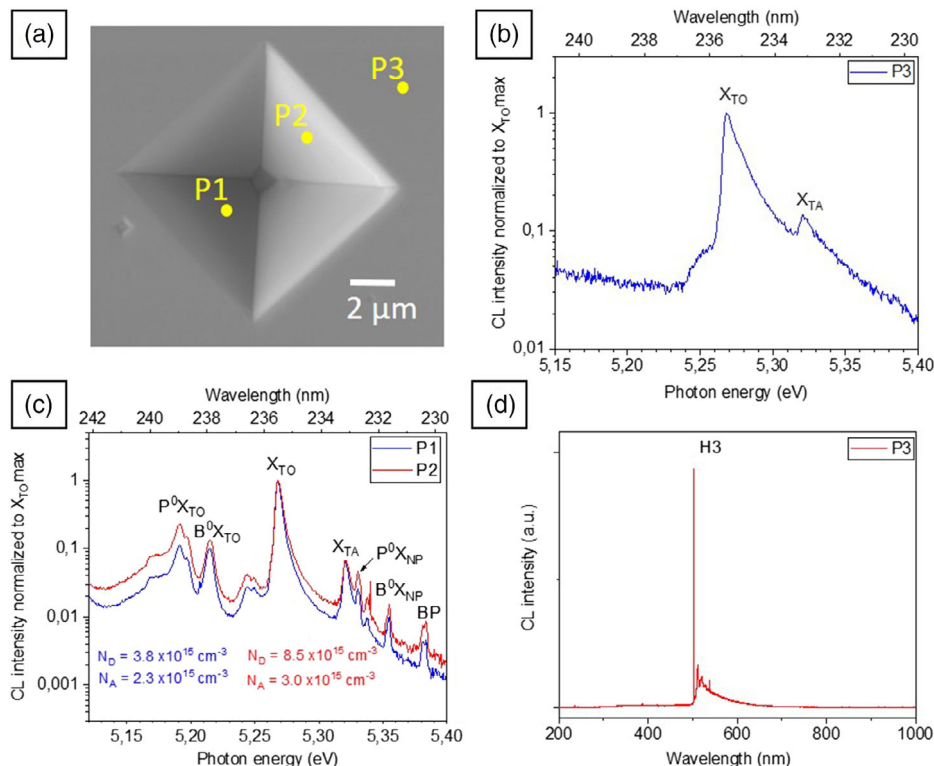


**Figure 5.** CL measurements on the V-shaped structure. a) SEM image with the labeled spots P1, P2, and P3, indicating where the CL spectra were obtained. b) CL spectrum on spot P3, showing only the free exciton lines  $X_{TO}$  and  $X_{TA}$ . c) CL spectra on spots P1 and P2, showing additional phosphorus- and boron-bound excitons ( $P^0X_{TO}$  and  $B^0X_{TO}$ ). d) UV-VIS CL spectrum on spot P3.

as  $N_A$ . The acceptor concentration  $N_A$  within the  $\{111\}$  facets was found to be low, in the range of  $N_A \approx 2 \times 10^{15} \text{ cm}^{-3}$ , which corresponds to the background concentration originating from the residual boron contamination in the reactor chamber. The maximum donor concentration  $N_D$  measured within  $\{111\}$  facets was  $N_D \approx 3 \times 10^{16} \text{ cm}^{-3}$ . As the donor concentration  $N_D$  was higher than the acceptor concentration  $N_A$ , the  $\{111\}$  facets of the inverted pyramidal and the umbrella-patterned structures can be considered to be n-type.

CL maps of the inverted pyramidal (Figure 6a) and of the umbrella-patterned (Figure 6b) structure display the spatial distribution of the donor and acceptor concentrations ( $N_D$  and  $N_A$ ), showing the enhanced incorporation of the dopants in the  $\{111\}$  facets and a clear contrast with respect to the dopant concentrations relative to the (100) area of the diamond surface and to the  $\{101\}$  facets of the umbrella-patterned structures, with the latter showing dopant concentrations that were approximately one order of magnitude smaller.

For the inverted pyramidal structure, the incorporation of phosphorus donors appeared quite homogeneous in the lower part, but with a higher concentration along the upper edges of the  $\{111\}$  facets. Like for the inverted pyramidal structure, the umbrella-shaped structure also exhibits a higher concentration along the upper edges of the  $\{111\}$  facets. This higher concentration along the upper edges of the  $\{111\}$  facets could be a morphological effect in the growth of an n-type layer on top of the catalytically etched structures. It is known that doping atoms are preferentially incorporated into step edges on the diamond surface. The AFM investigations show that the angle of inclination of the pyramid surfaces near the edge decreases slightly. Due to this deviation from an ideal  $\{111\}$  facet, atomic

steps are created in this area, which are known to favor the incorporation of dopants. This effect for phosphorus incorporation can be very nicely seen in a CL map in the publication of Pinault-Thaury et al.<sup>[29]</sup>

Temahuki et al.<sup>[20]</sup> proved via secondary ion mass spectroscopy (SIMS) that the P-concentration within the V-shapes is higher than on the (100) surface, but they could not resolve the doping distribution spatially because of the low spatial resolution of the SIMS equipment and the small sizes of the V-shapes, which were in the order of 200–400 nm. Thus, our results show the high-resolution doping concentration distributions on the different facets of the Ni-etched and overgrown structures.

### 3. Conclusion

In summary, our results showed the high-resolution doping concentration distribution on different facets of Ni-etched structures overgrown with an n-type doped diamond film. We demonstrated the enhancement of the P-concentration on (100) diamond samples by selectively overgrowing the  $\{111\}$  facets of inverted pyramidal structures that were produced by a catalytic etching process that used Ni in a hydrogen atmosphere at elevated temperatures. This method may overcome the limitations associated with low doping efficiencies in the growth of (100) diamond samples, and thus facilitate the fabrication of (100) diamond power devices with low on-resistances and better Ohmic contact performances. Future work should explore methods to increase the phosphorus concentration and to optimize its incorporation distribution on the  $\{111\}$  facets. The degrees of

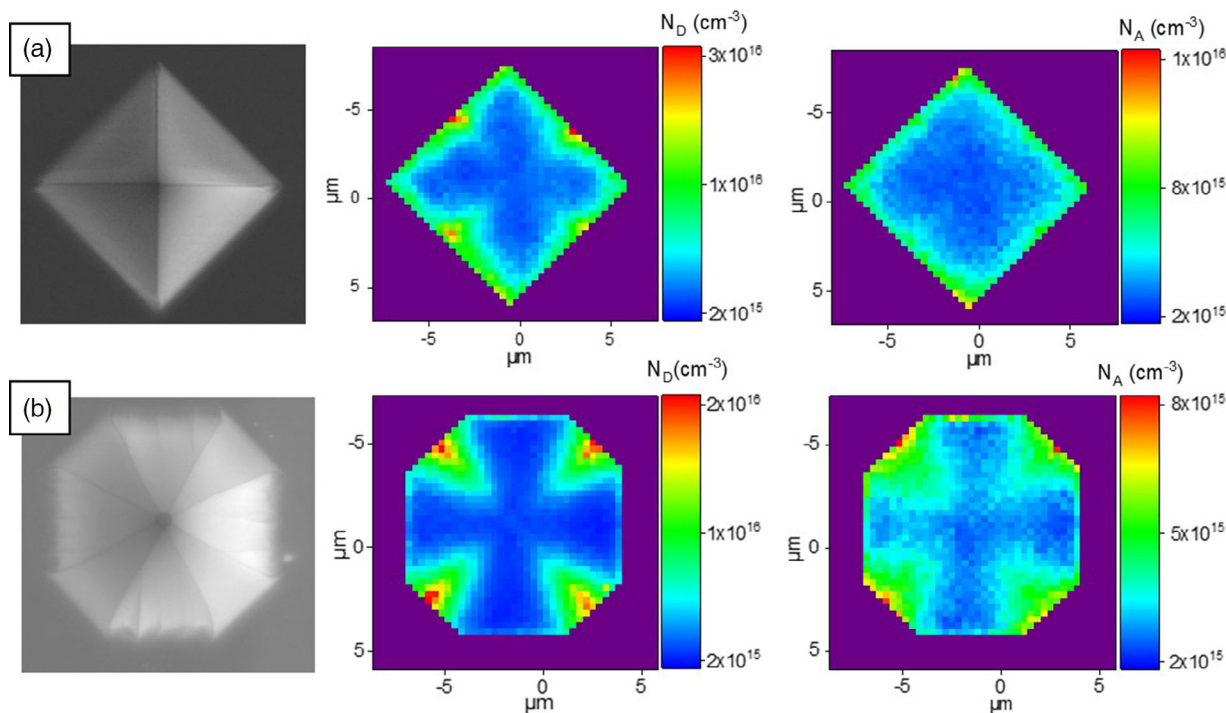


**Figure 6.** CL map of a) the square-shaped and b) the umbrella-patterned structures displaying the spatial distribution of the donor and acceptor concentrations, which show the enhanced incorporation of the dopants in the  $\{111\}$  facets.

freedom for the lithography of Ni masks offer flexibility with respect to the design of n-type V-shaped structures. The dimensions (lateral size and depth) of these trench structures can be defined exactly by simply defining the lateral dimensions of the Ni mask deposited on the diamond surface and the duration of the subsequent etching process. To achieve optimum results, i.e., perfectly shaped inverted pyramidal structures via catalytic etching, the edges of the Ni masks must be aligned along the  $\langle 110 \rangle$  crystallographic direction of the diamond sample.

#### 4. Experimental Section

Synthetic and double-side polished (100) Ib-type HPHT diamond substrates with dimensions of  $4 \times 4 \times 0.5$  mm were purchased from a commercial supplier (Sumitomo). First, the substrates were cleaned in nitric acid ( $\text{H}_2\text{SO}_4 + \text{HNO}_3$  at a ratio of 3:1) at  $220^\circ\text{C}$  to remove all graphitic and metallic residuals on the surface. We selected Ni as the catalyst because it is the candidate metal with the highest carbon solubility and, therefore, the highest etching activity. Ni masks with a thickness of 200 nm were deposited on the diamond surface using photolithography and electron beam evaporation. Square-shaped masks with areas of  $5 \times 5 \mu\text{m}$  and  $10 \times 10 \mu\text{m}$  were deposited. The edges of the deposited Ni masks were aligned either along the  $\langle 110 \rangle$  or the  $\langle 100 \rangle$  direction. Catalytic etching was performed in an induction furnace with a base pressure of  $10^{-6}$  mbar. For the etching procedure, we introduced hydrogen with a flow and pressure of 100 sccm and 500 mbar, respectively. The temperature was raised to  $850^\circ\text{C}$  at a rate of  $150 \text{ K min}^{-1}$ , measured with a pyrometer with a reading precision of  $\pm 5$  K. After etching, the samples were cooled for 1 h under continuous hydrogen flow. Next, the residual Ni and graphite were removed from the diamond surface via immersion in an acid mixture. These etching parameters were the result of optimization experiments investigating diamond etching with Ni, which will be published elsewhere in the future.

For the subsequent overgrowth of the V-shapes with an n-type diamond film, we used a home-built chemical vapor deposition (CVD) reactor system.<sup>[30]</sup> Prior to overgrowth, the sample was pretreated for 3 min in pure hydrogen plasma at 3 kW and 200 mbar to clean the surface and achieve an appropriate growth temperature. The pretreatment step was as short as possible to prevent strong surface roughening due to plasma etching. After the pretreatment step, we used a low  $\text{CH}_4/\text{H}_2$  ratio of 0.2% to obtain a low growth rate to ensure that the deposited film was of high quality and the inverted pyramids were not filled completely by the overgrown film. To dope the film with phosphorus, we used trimethylphosphine  $\text{P}(\text{CH}_3)_3$  (TMP) as a gas source, which was added to the aforementioned  $\text{CH}_4/\text{H}_2$  gas in the reactor chamber using a  $\text{P}/\text{CH}_4$  ratio of 4.4%. This value is in the upper range typically used for doping (100) and (111) diamond,<sup>[4]</sup> but due to our current mass flow controller configuration and the concentration of TMP in the gas supply (1% TMP mixed in pure  $\text{H}_2$  filled in a gas bottle) at our CVD reactor system, it is not possible to reach much lower  $\text{P}/\text{CH}_4$  ratios. To increase the doping efficiency, we increased the deposition pressure to 260 mbar, keeping the microwave power at 3 kW, resulting in a substrate temperature of  $980^\circ\text{C}$ , which is higher than that required for the growth of intrinsic diamond ( $\approx 800^\circ\text{C}$ ). This higher temperature is in accordance with reported deposition temperature ranges used for n-type doping.<sup>[3–6]</sup>

With these parameters, the growth rate on the (111)-oriented surfaces was  $\approx 100 \text{ nm h}^{-1}$ , and the deposition time was 8 h, resulting in a film thickness of  $\approx 800$  nm on the {111} facets. After overgrowth, we cleaned the samples in an acid mixture to remove graphite from the surface.

To measure the dimensions and investigate the quality of the etched and overgrown structures, we used a WLI (Bruker Contour GT), an AFM (Bruker Dimension Icon), and a SEM (Zeiss Auriga Crossbeam).

CL characterization was performed to assess the phosphorus concentration on the different facets of the n-type doped V-shaped structures. A JEOL 7001F field emission-SEM with an optical detection system was used to collect CL spectra with high spatial and spectral resolution in the UV range.<sup>[31]</sup> An acceleration voltage of 5 kV was applied, corresponding to the

stopping depth for electrons at  $\approx 200 \text{ nm}$ .<sup>[32]</sup> To resolve the lines of both the free and bound excitons in the UV range, a requirement to determine the dopant concentrations, the samples were cooled down to  $\approx 7$  K using liquid helium. The intensity ratio between the lines of bound and free excitons is proportional to the concentration of the dopant in the film. The quantification of the electrically active phosphorus atoms (donors) in the films was performed using a reference sample measured under identical conditions. This method can be applied to a wide range of dopant concentrations in diamond down to  $\approx 10^{12} \text{ cm}^{-3}$ , which makes CL spectroscopy a highly sensitive tool for the quantification of dopants in diamond, surpassing the detection limits of SIMS. Details describing the use of CL spectroscopy for measuring the concentration of dopants in diamond can be found in the literature.<sup>[23,24,32]</sup>

#### Acknowledgements

The authors gratefully acknowledge the financial support from the European Union's Horizon 2020 research and innovation program under grant no. SEP-210184415 (GreenDiamond).

Open access funding enabled and organized by Projekt DEAL.

#### Conflict of Interest

The authors declare no conflict of interest.

#### Data Availability Statement

Research data are not shared.

#### Keywords

catalytic etching, cathodoluminescence, diamond, n-type doping, phosphorus

Received: August 5, 2020

Revised: December 31, 2020

Published online: February 17, 2021

- [1] A. Fiori, T. Teraji, Y. Koide, *Appl. Phys. Lett.* **2014**, *105*, 133515.
- [2] H. Umezawa, Y. Kato, S. Shikata, *Appl. Phys. Express* **2013**, *6*, 011302.
- [3] T. Makino, N. Tokuda, H. Kato, M. Ogura, M. Watanabe, S.-G. Ri, S. Yamasaki, H. Okushi, *Jpn. J. Appl. Phys.* **2006**, *45*, L1402.
- [4] H. Kato, T. Makino, S. Yamasaki, H. Okushi, *J. Phys. D: Appl. Phys.* **2007**, *40*, 6189.
- [5] S. Koizumi, M. Kamo, Y. Sato, H. Ozaki, T. Inuzuka, *Appl. Phys. Lett.* **1997**, *71*, 1065.
- [6] H. Kato, S. Yamasaki, H. Okushi, *Appl. Phys. Lett.* **2005**, *86*, 222111.
- [7] S. Koizumi, H. Umezawa, J. Pernot, M. Suzuki, *Power Electronics Device Applications of Diamond Semiconductors*, Woodhead Publishing, Duxford **2018**, pp. 1–97.
- [8] M. Schreck, S. Gsell, R. Brescia, M. Fischer, *Sci. Rep.* **2017**, *7*, 44462.
- [9] J. P. Goss, R. Jones, M. I. Heggie, C. P. Ewels, P. R. Briddon, S. Öberg, *Phys. Rev. B* **2002**, *65*, 115207.
- [10] L. G. Wang, A. Zunger, *Phys. Rev. B: Condens. Matter Mater. Phys.* **2002**, *66*, 1.
- [11] S. Koizumi, M. Suzuki, *Phys. Status Solidi A* **2006**, *203*, 3358.
- [12] M. De Feudis, V. Mille, A. Valentin, O. Brinza, A. Tallaire, A. Tardieu, R. Issaoui, J. Achard, *Diam. Relat. Mater.* **2019**, *92*, 18.
- [13] H. Kato, T. Makino, M. Ogura, N. Tokuda, H. Okushi, S. Yamasaki, *Appl. Phys. Express* **2009**, *2*, 055502.



- [14] Y. Kawabata, J. Taniguchi, I. Miyamoto, *Diam. Relat. Mater.* **2004**, 13, 93.
- [15] D. T. Tran, C. Fansler, T. A. Grotjohn, D. K. Reinhard, J. Asmussen, *Diam. Relat. Mater.* **2010**, 19, 778.
- [16] W. Smirnov, J. J. Hees, D. Brink, W. Müller-Sebert, A. Kriele, O. A. Williams, C. E. Nebel, *Appl. Phys. Lett.* **2010**, 97, 073117.
- [17] H. Al Mehedi, J.-C. Arnault, D. Eon, C. Hébert, D. Carole, F. Omnes, E. Gheeraert, *Carbon* **2013**, 59, 448.
- [18] Y. Morofushi, H. Matsushita, N. Miki, *Precis. Eng.* **2011**, 35, 490.
- [19] T. Ohashi, W. Sugimoto, Y. Takasu, *Diam. Relat. Mater.* **2011**, 20, 1165.
- [20] N. Temahuki, R. Gillet, V. Sallet, F. Jomard, E. Chikoidze, Y. Dumont, M.-A. Pinault-Thaury, J. Barjon, *Phys. Status Solidi A* **2017**, 214, 1700466.
- [21] M. Nagai, K. Nakanishi, H. Takahashi, H. Kato, T. Makino, S. Yamasaki, T. Matsumoto, T. Inokuma, N. Tokuda, *Sci. Rep.* **2018**, 8, 6687.
- [22] J. Achard, S. Silva, O. Brinza, X. Bonnin, V. Mille, R. Issaoui, M. Kasu, A. Gicquel, *Phys. Status Solidi A* **2009**, 206, 1949.
- [23] J. Barjon, *Phys. Status Solidi A* **2017**, 214, 1700402.
- [24] J. Barjon, P. Desfonds, M. A. Pinault, T. Kociniewski, F. Jomard, J. Chevallier, *J. Appl. Phys.* **2007**, 101, 113520.
- [25] M. Nesladek, *Semicond. Sci. Technol.* **2005**, 20, R19.
- [26] J.-H. Hsu, W.-D. Su, K.-L. Yang, Y.-K. Tzeng, H.-C. Chang, *Appl. Phys. Lett.* **2011**, 98, 193116.
- [27] C. J. Widmann, W. Müller-Sebert, N. Lang, C. E. Nebel, *Diam. Relat. Mater.* **2016**, 64, 1.
- [28] F. Silva, X. Bonnin, J. Achard, O. Brinza, A. Michau, A. Gicquel, *J. Cryst. Growth* **2008**, 310, 187.
- [29] M.-A. Pinault-Thaury, T. Tillocher, D. Kobor, N. Habka, F. Jomard, J. Chevallier, J. Barjon, *J. Cryst. Growth* **2011**, 335, 31.
- [30] M. Fuener, C. Wild, P. Koidl, *Appl. Phys. Lett.* **1998**, 72, 1149.
- [31] H. Bensalah, I. Stenger, G. Sakr, J. Barjon, R. Bachelet, A. Tallaire, J. Achard, N. Vaissiere, K.-H. Lee, S. Saada, J.-C. Arnault, *Diam. Relat. Mater.* **2016**, 66, 188.
- [32] S. Koizumi, H. Umezawa, J. Pernot, M. Suzuki, *Power Electronics Device Applications of Diamond Semiconductors*, Elsevier, San Diego, CA **2018**.